Further Rotation Reversal Studies in C-Mod L-mode Plasmas

J.E. Rice[‡], N.M. Cao[†], P.H. Diamond[♯], M.J. Greenwald[‡],

A.E. Hubbard[‡], E.S. Marmar[‡], M.L. Reinke [♮] and P. Rodriguez-Fernandez[‡]

[‡]*PSFC MIT, Cambridge, Massachusetts 02139, USA*

[†]*CIMS NYU, New York, New York 10012 USA*

[♯]*UCSD, La Jolla, California 92093, USA*

[♮]*CFS, Cambridge, Massachusetts 02139, USA*

corresponding author: J.E. Rice rice@psfc.mit.edu

Abstract

Studies of core toroidal rotation reversal phenomenology in C-Mod deuterium L-mode plasmas have been expanded to include details of the dependences on plasma current and toroidal magnetic field. Rotation reversal occurs at a critical density and universal scaling indicates that the product of $n_{crit} q_{95} R \sim B_T/2$, with n_{crit} in $10^{20}/m^3$, R in m and B_T in T. Measurements in H and He plasmas exhibit similar behavior, including a connexion with the LOC/SOC transition and the cut-off for non-diffusive heat transport. Electron density and ICRF power modulation experiments suggest that the collisionality ν_* is a unifying parameter. Strong impurity puffing causes the critical density to increase, indicating that the situation is more complicated than only collisionality, perhaps involving the details of the effects of dilution on ITG mode stability.

1. Introduction

Rotation reversal, the change in sign of the core toroidal velocity, has been widely observed in tokamak Ohmic L-mode discharges [1]. While some authors favor a general definition of reversals to be parameterized by changes in the velocity gradient at mid radius, a change in sign of the core intrinsic rotation is indicative of a change in sign of the residual stress, and only the Type I reversals [1] will be discussed here. Clearly if the core velocity changes sign while the edge rotation is held fixed (as in Type I reversals), there must also be a variation in the mid radius gradient. However, the velocity gradient can change due to the momentum pinch, but a change in sign in the core rotation can only be through a change in sign of the residual stress [2] (if the edge rotation remains fixed), and it is the latter case which is of interest here. Rotation reversals were first seen through changes in the electron density, either dynamically *via* density ramping [3, 4, 5, 6, 7, 8, 9, 10, 11, 12, 13, 14, 15, 16, 17, 18, 19] or from shot to shot scans [5, 6, 7, 8, 10, 11, 13, 20, 15, 21]. There is a critical density for rotation reversal which increases with plasma current at fixed magnetic field [6, 8, 10, 11] and the rotation velocity is anti-correlated with B_T [7, 8, 10]. There exists hysteresis between the electron density and the core rotation velocity [4, 6, 8, 17, 19], with both co- and counter-current rotation states for the same density. This is *prima facie* evidence of bifurcation and a first order transition. Rotation reversals are accompanied by changes in turbulence [8, 9, 10, 11, 13, 14, 20, 22, 23, 16, 17, 19], and have been associated with Ohmic energy confinement saturation [8, 10, 11, 12, 13, 20, 22, 15, 16, 17, 19, 24] and cut-off of non-diffusive heat transport (formerly called 'non-local' cut-off) [11, 13, 22, 24]. Gyro-kinetic modeling suggests that in the low density co-current rotation state, TEM turbulence is important while at high density, with counter-current rotation, ITG modes dominate [10, 12, 13, 20, 1, 22, 23, 16, 17, 19].

The present study, which seeks to expand on this body of information, was conducted on the C-Mod tokamak [25, 26], a compact (minor radius $a \sim 0.21$ m, major radius R = 0.67 m), high field device ($B_T \leq 8.1$ T) with the usual shaping capabilities and complement of diagnostics [27]. Core toroidal rotation velocity (V_ϕ) spatial profiles were obtained with an imaging x-ray crystal spectrometer in the Johann configuration [28, 29] viewing H- and He-like argon. In section 2 will be presented the dependence of V_ϕ on plasma current and toroidal magnetic field in deuterium plasmas, along with scalings of the critical density for rotation reversal and its relation to the density limit. Results for hydrogen and helium discharges will also be demonstrated. The subject of section 3 will be electron density and ICRF power modulation experiments, along with the effects of strong impurity puffing on rotation reversals, and an attempt at unifying results through the collisionality. Section 4 will include a discussion and summary.

2. Scalings of Rotation Reversals with Plasma Current and Magnetic Field

In this section, the relationship between rotation reversals and these plasma parameters will be explored: electron density, plasma current and toroidal magnetic field. Shown in Fig.1 are parameter time histories of a 5.4 T, 1.2 MA ($q_{95} \sim 3.3$) D dis-

charge with a slight downward density ramp. The rotation switched from counter- to

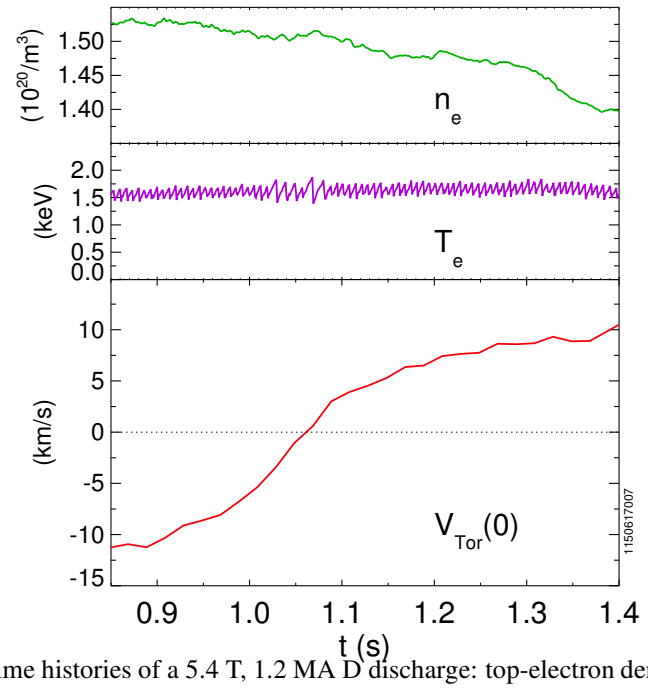

Figure 1: Time histories of a 5.4 T, 1.2 MA D discharge: top-electron density, middle-central electron temperature, bottom- central toroidal rotation velocity.

co-current for a line-averaged density around 1.5×10^{20}/m^3. A series of individual 1.2 MA discharges confirms this critical density, as is demonstrated in Fig.2. Similar density scans have been performed for a wide range of plasma currents, from 0.4 to 1.2 MA, for D discharges at fixed magnetic field (5.2-5.5 T), and the results for the critical density are shown in the top frame of Fig.3. The dashed line in the top frame represents the best linear fit. Shown in the middle frame is the critical density for the LOC/SOC transition, which similarly increases with plasma current [30, 8, 10, 11, 24]. In the bottom frame is the cut-off density for non-diffusive heat transport, again showing a similar scaling with current [11, 24].

The dependence of rotation reversals on the toroidal magnetic field has also been investigated, and at fixed density, changes in B_T can induce rotation reversals. Shown in Fig.4 are parameter time histories of a discharge with toroidal magnetic field modulation, and with the electron density held constant. There is an anti-correlation between the magnetic field and the central rotation velocity [7, 8, 10], with a slight delay of about a momentum confinement time. For this 0.8 MA discharge ($q_{95} \sim 4.8$) with n_e $\sim7.7\times10^{19}$/m^3, the rotation reversal occured for $B_T \sim 5.3$ T. This anti-correlation is emphasized in Fig.5 which shows two discharge trajectories in the B_T-V_ϕ plane resulting from magentic field modulations. This doesn't exhibit strong hysteresis [8] as has

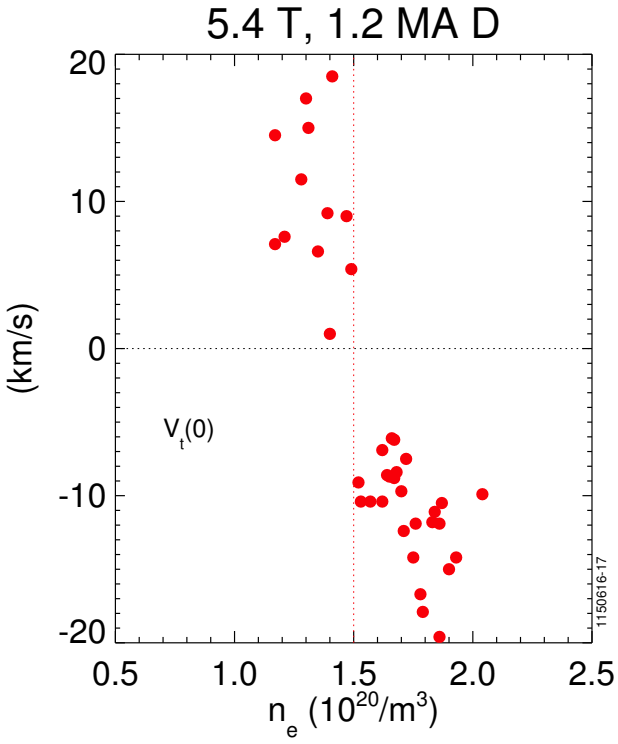

Figure 2: The core toroidal rotation velocity as a function of electron density for a series of 1.2 MA, 5.4 T deuterium discharges.

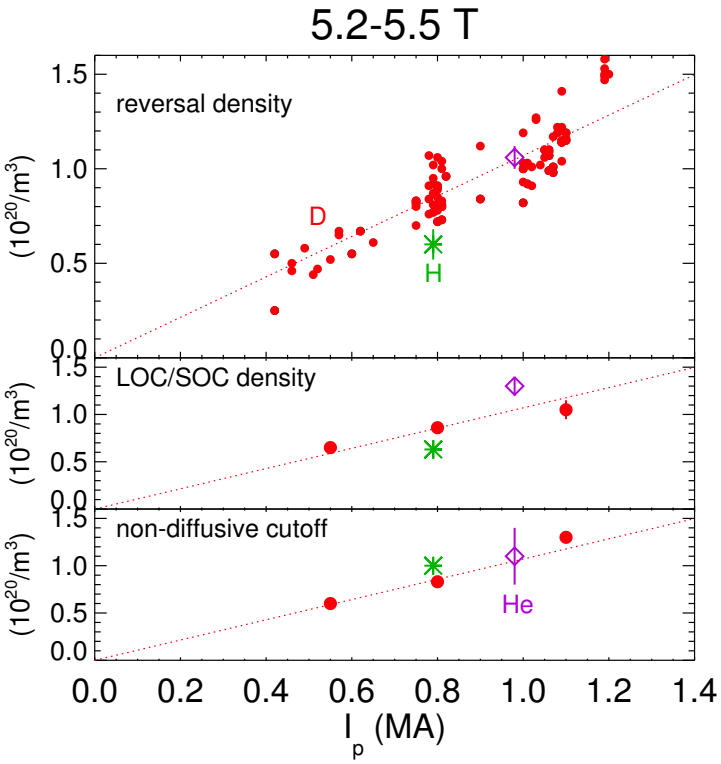

Figure 3: Plasma current scaling of the critical densities for rotation reversal (top frame), the LOC/SOC transition (middle frame and non-diffusive cut-off (bottom frame) for plasmas with toroidal magnetic field between 5.2 and 5.5 T. Red dots: D, green asterisks: H, purple diamonds: He. The red dotted line in the top frame is the best linear fit for the D points, and has been reproduced in the other frames.

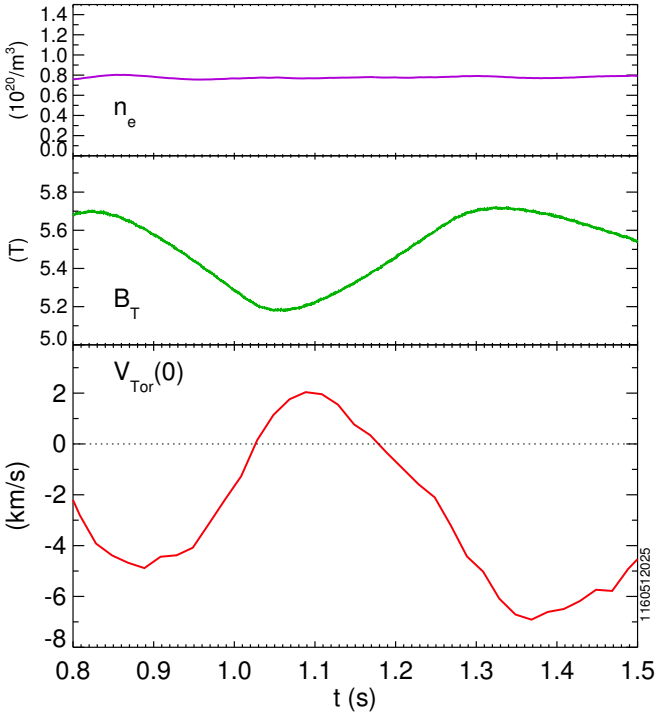

Figure 4: Time histories of a 0.8 MA D discharge with toroidal magnetic field modulation. Top frame- electron density, middle frame- magnetic field, bottom frame- core toroidal rotation velocity.

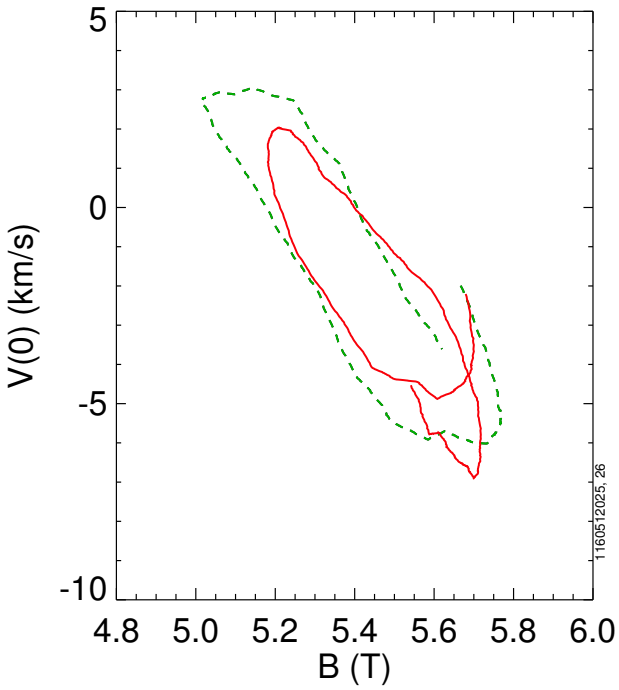

Figure 5: Trajectories in the B_T-V_ϕ plane for two 0.8 MA D discharges at n_e $\sim 7.7 \times 10^{19}/m^3$ with magnetic field modulations.

been seen with density modulation (see Fig.14), and the width of the loop is due to a finite momentum confinement time, which is about 35 ms [31].

It's clear that both the plasma current and the toroidal magnetic field influence the rotation reversal process. In order to unravel the dependences, consider the comparison of two discharges with $q_{95} \sim 3.9$ (one at 1.4 MA and 7.8 T, the other at 0.7 MA and 3.9 T) shown in Fig.6. The rotation reversal occured at a density of 1.64×10^{20}/m^3 for

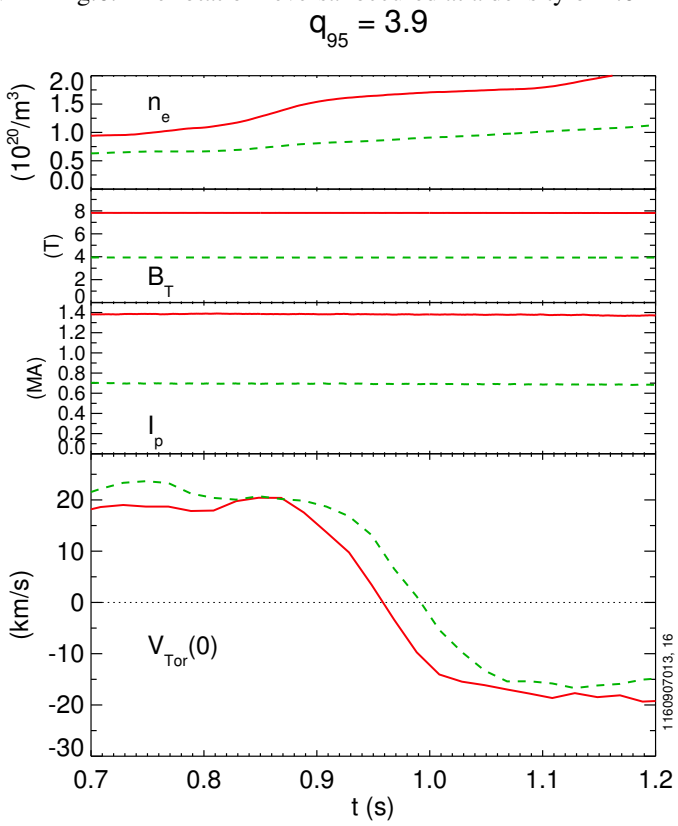

Figure 6: Time history comparison of two D discharges with q_{95} = 3.9, solid red- 1.4 MA, 7.8 T; dashed green- 0.7 MA, 3.9 T. Top frame- electron density, second frame- toroidal magnetic field, third frame- plasma current, bottom frame- central toroidal rotation velocity.

the 7.8 T discharge (red) and 0.88×10^{20}/m^3 for the other at 3.9 T (green dashed). This indicates that the product of the critical density and q_{95} scales with B_T [24]. This is explicitly shown in Fig.7 for a database of over 100 C-Mod deuterium discharges (R = 0.67 m). Rotation reversal occurs when $n_{crit}q_{95}R/B \sim 1/2$, with n_{crit} in 10^{20}/m^3, B in T and R in m. Admittedly, it's not possible to determine the scaling with major radius R from measurements on a single device. That information is available from observations from multiple tokamaks [24] and is shown in Fig.8. The red dots depict rotation reversals from 5 individual machines, which align very closely with the C-Mod

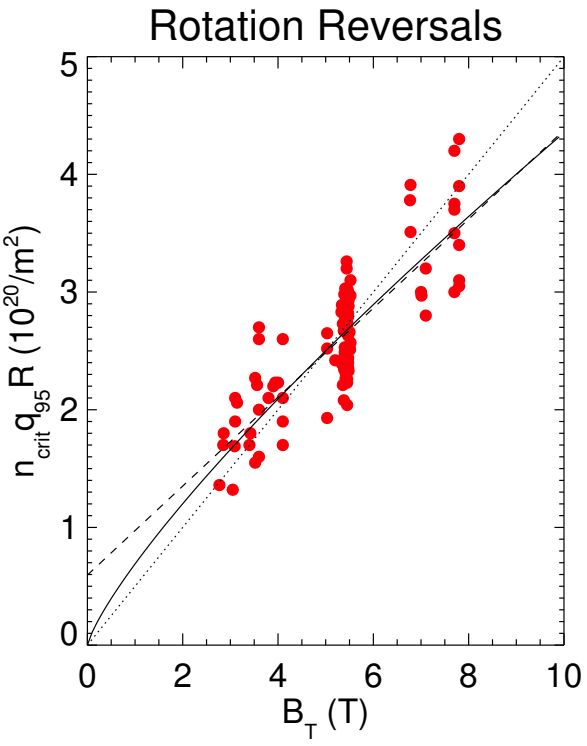

Figure 7: The product $n_{crit}q_{95}R$ for rotation reversals as a function of toroidal magnetic field for C-Mod D discharges. The dashed line is the best linear fit, the solid line is $\propto B^{0.8}$ and the dotted line represents $n_{crit}q_{95}R/B = 1/2$.

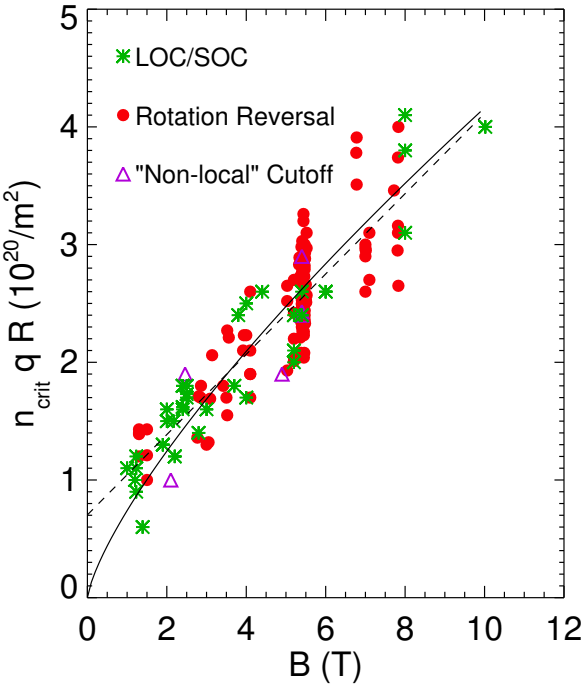

Figure 8: The product $n_{crit}q_{95}R$ as a function of toroidal magnetic field for discharges from 18 different devices: green asterisks- the LOC/SOC transition, red dots- rotation reversal, purple triangles- non-diffusive cut-off. The dashed line is the best linear fit and the solid line is $\propto B^{0.75}$.

results, validating the scaling with R. These points demonstrate a range of R from 0.67 to 1.8 m. There is an apparent connection among rotation reversals, the LOC/SOC transition and the so-called 'non-local' cut-off in cold pulse propagation experiments [8, 9, 10, 11, 24], which allows further expansion in the range of R (0.64 to 3.1 m) and B_T (1 to 10 T). The values of the product $n_{crit}q_{95}R$ for the LOC/SOC transition from 16 devices are shown by the green asterisks and for the non-diffusive cut-off (4 tokamaks) by the purple triangles [24]. There is a clear trend in these points, further bolstering the scaling $n_{crit}q_{95}R/B \sim 1/2$.

This condition may be recast using the approximation $q_{95} \approx 2\pi Ba^2(1+\kappa^2)/2\mu_0 RI_p$ [32], where κ is the elongation, with B in T, a and R in m and I_p in MA. Recognizing that the density limit is defined as $n_G \equiv I_p/\pi a^2$ [33], the critical condition becomes (taking $\kappa \sim 1.6$, which is typical for C-Mod) $n/n_G \sim 1/6$. A database of C-Mod rotation reversals has been assembled from discharges with the plasma current in the interval from 0.40 to 1.57 MA, with toroidal magnetic field between 2.9 and 8.1 T. The corresponding range in the critical density spanned a factor of 4, from 0.43 to $1.85\times10^{20}/m^3$. The statistics for C-Mod rotation reversals are presented in the top frame of Fig.9, which indicate a sharp peak near $n/n_G \sim 0.15$, in good agreement with the preceding algebra. For the LOC/SOC transitions from multiple devices [24], there is a much broader distribution with n/n_G, extending from 0.1 to 0.5, as can be seen in the bottom frame. This apparent discrepancy compared to the results of Figs.7 and 8 can be traced to two causes. Most of the LOC/SOC points in Fig.8 were from older devices with circular plasmas, which reduces the contribution from the elongation (thereby increasing n/n_G) by about a factor of 2 compared to C-Mod with κ = 1.6. Furthermore, the range in inverse aspect ratio for the multiple devices extended from 0.20 to 0.33, so the dimensional contribution of R (in Fig.8) is not the same as the contribution of a in n/n_G.

The previous results were from C-Mod deuterium (D) plasmas. Similar studies on rotation reversals and Ohmic confinement saturation have recently been conducted in hydrogen (H), tritium (T) and helium (He) plasmas [34, 35]. Shown in Fig.10 are density scans from 5.4 T, 0.8 MA H discharges in C-Mod. In the top frame is the global energy cofinement time, with the usual LOC region at low density (solid line) and with SOC at high density (dashed line). The critical density for the LOC/SOC transition is somewhere in the interval 6-$7\times10^{19}/m^3$. In the bottom frame is the core toroidal rotation velocity, with the reversal occurring near $5\times10^{19}/m^3$. In the middle frame, the transition between non-diffusive and diffusive heat transport following cold pulses is about $1\times10^{20}/m^3$. Although these three transitions are not precisely aligned, they are certainly within the scatter of the D results, as can by seen by examination of the H points (green asterisks) in Fig.3. Similar experiments have been performed in He plasmas, and the results are presented in Fig.11 for 5.4 T, 1.0 MA discharges. At this higher current, the LOC/SOC transition (top) and rotation reversal (bottom) occur at higher density. Unfortunately for the non-diffusive cut-off (middle), there are only two measurements, one deep in the LOC regime and the other deep into SOC. These points have also been included in Fig.3 as purple diamonds. The main takeaway is that in the big picture, there aren't substantial differences for these three phenomena in H, D and He working gases, although wide ranging studies have not been performed for H

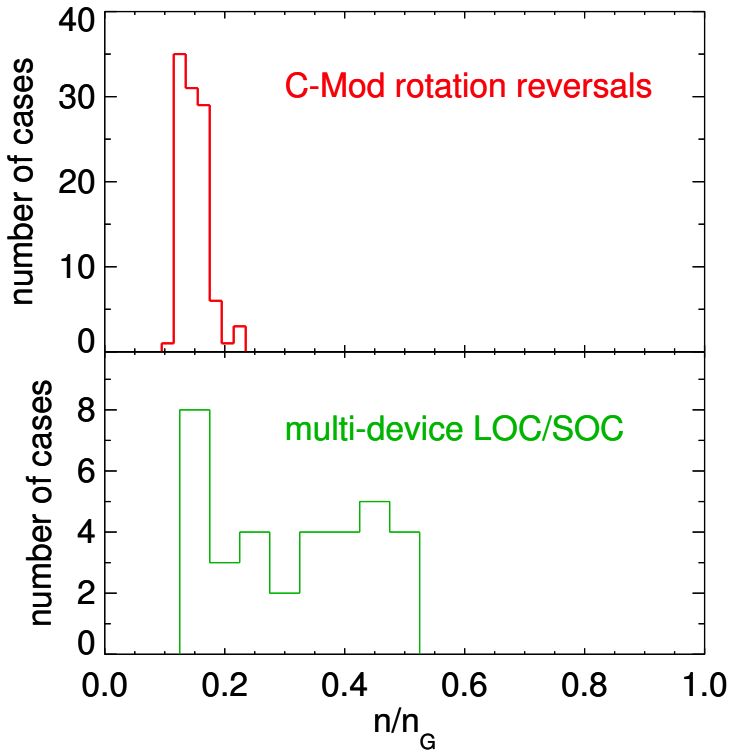

Figure 9: Histograms of the number of C-Mod rotation reversals (top frame) and LOC/SOC transitions from multiple devices (bottom frame) as a function of the normalized density, n/n_G.

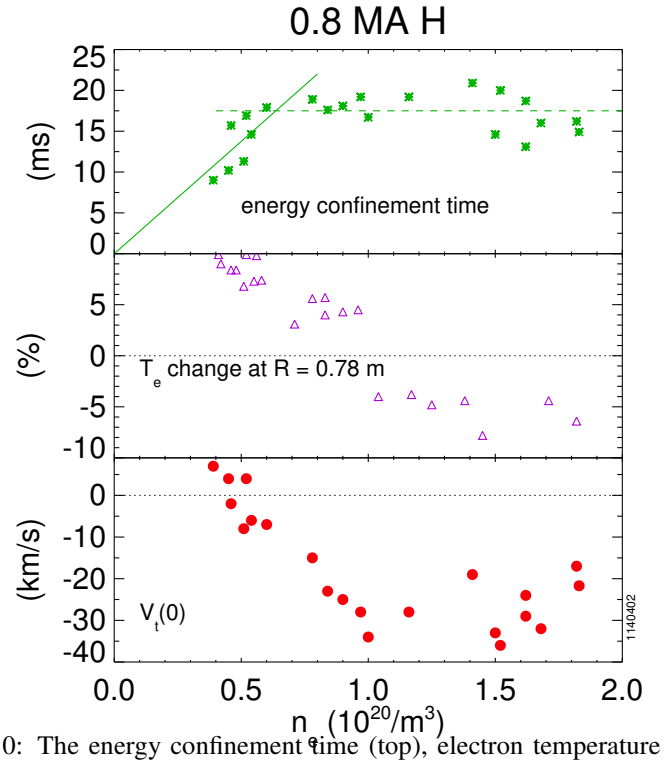

Figure 10: The energy confinement time (top), electron temperature change at R = 0.78 m following an edge cold pulse (middle) and the core toroidal rotation velocity (bottom) as a function of electron density for 5.4 T, 0.8 MA H discharges.

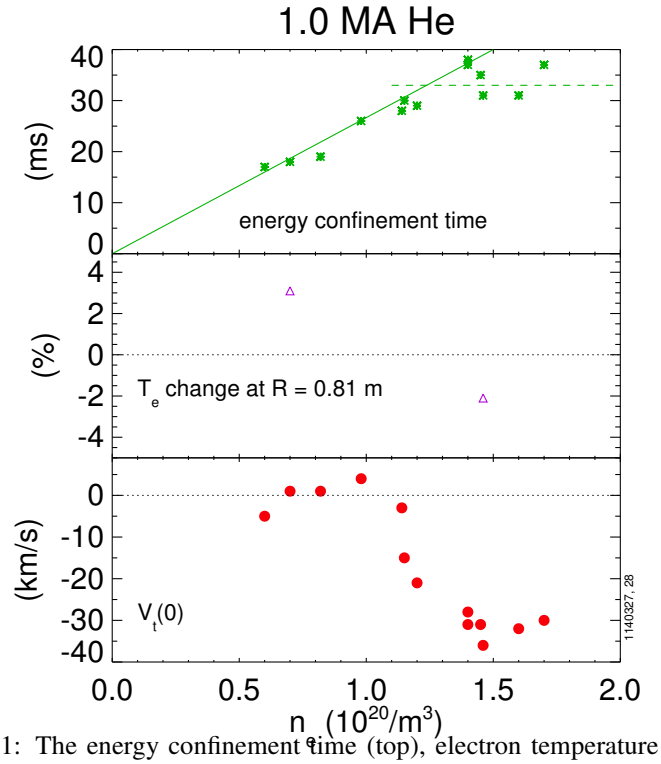

Figure 11: The energy confinement time (top), electron temperature change at R = 0.81 m following an edge cold pulse (middle) and the core toroidal rotation velocity (bottom) as a function of electron density for 5.4 T, 1.0 MA He discharges.

or He plasmas. It is possible that the LOC/SOC critical density increases slightly with background ion mass, which is similar to the results from other devices [34, 35].

3. Modulation Experiments, Strong Impurity Puffing and the Role of Collisionality in Rotation Reversals

The previous section was concerned mainly with parameter scalings of rotation reversals depending upon electron density, plasma current and toroidal magnetic field. In addition, modulation of B_T was executed, which revealed a mostly inverse relation between B_T and V_ϕ, without evidence for hysteresis. Further modulation experiments have been performed, of the electron density and electron temperature (through the ICRF power). An example of varying the density [8, 19] is shown in Fig.12. The top

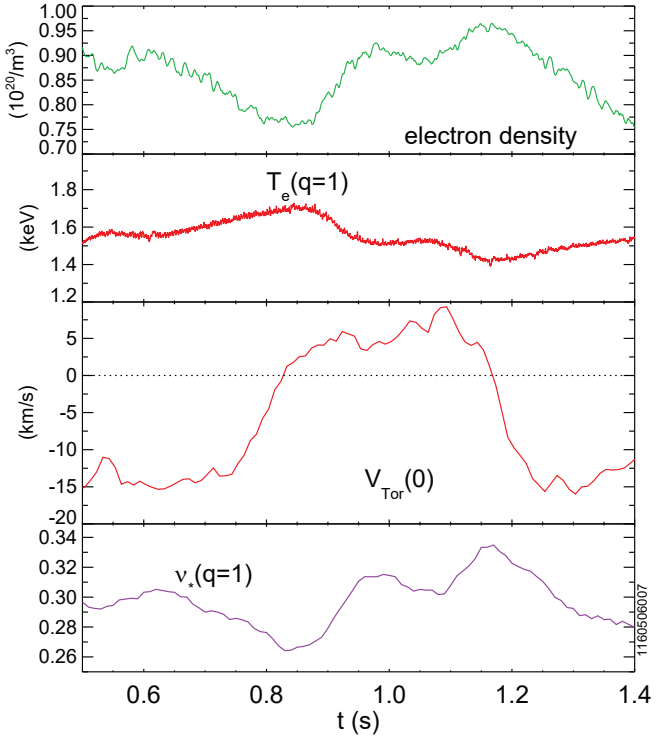

Figure 12: Time histories of a 5.5 T, 0.8 MA D discharge with a density modulation. Top- electron density, second frame- electron temperature at the q=1 surface, third frame- core toroidal rotation velocity, bottom- collisionality ν_* at the q = 1 surface.

frame shows the density modulation, $\pm$ 15%, in the vicinity of the critical density. The response of the core velocity (third frame) indicates hysteresis [8, 19] since both co-

and counter-current rotation states are seen for the same electron density. In the second frame is shown the electron temperature near the q = 1 surface (in order to avoid the effects of sawteeth), and in the bottom frame is the collisionality ν_*, evaluated at the q = 1 surface. There was some earlier speculation that ν_* is an important parameter for rotation reversal [8, 10], and that hypothesis can be tested with auxiliary heating at fixed density, while varying the collisionality through its dependence on electron temperature. The use of ECH to change ν_* (through its dependence on temperature) in rotation reversal experiments has been demonstrated [22, 16]. The rotation profile characteristics with ICRF heating (mainly to electrons) on C-Mod have been previously shown to be similar to Ohmic plasmas as long as the power is low enough to stay out of H- or I-mode [36, 37, 38], typically achieved in the unfavorable ∇B drift configuration. Shown in Fig.13 are parameter time histories for a C-Mod discharge with rotation reversals induced by ICRF power modulation (and hence electron temperature modulation) at a fixed density. The response of the core rotation velocity is

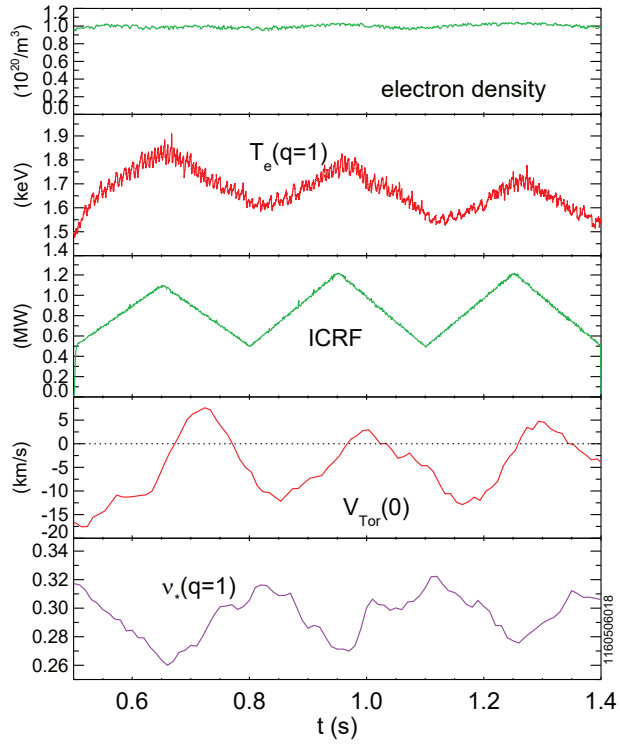

Figure 13: Time histories of a 5.5 T, 0.8 MA D discharge with ICRF power modulation. Top- electron density, second frame- electron temperature at the q = 1 surface, third frame- ICRF power, fourth frame- core toroidal rotation velocity, bottom- collisionality ν_* at the q = 1 surface.

substantially delayed relative to the ICRF modulation, and again there is evidence for hysteresis since both co- and counter-current rotation states exist for the same electron temperature (second frame) or collisionality (bottom frame), evaluated at the q = 1 surface. The results of Figs.12 and 13 can be unified by looking at the discharge trajectories in the ν_*-V_ϕ plane, as is demonstrated in Fig.14. In these cases there is a true

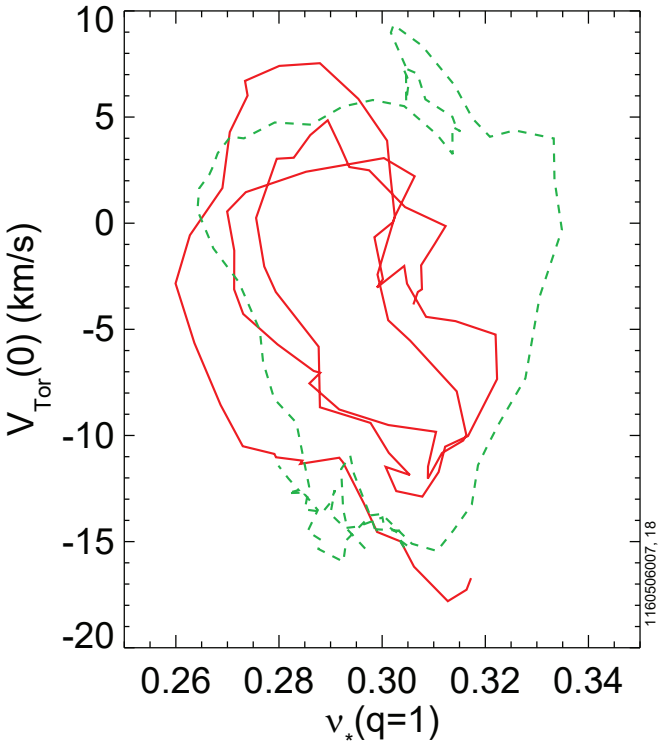

Figure 14: Discharge trajectories in the ν_*-V_ϕ plane for the plasmas of Fig.12 (density modulation, green dashed line) and Fig.13 (ICRF power modulation, solid red line).

hysteresis loop (in contrast to Fig.5), and for both plasmas, the co- and counter-current rotation states exist for the same collisionality, $\nu_* \sim 0.3$ (at the q = 1 surface). The overlap of the loops for both discharges suggests that the collisionality is a unifying parameter. Similar values for the critical collisionality for rotation reversals and the LOC/SOC transition have been observed on multiple devices [24].

The collisionality can also be changed through its dependence on $Z_{\rm eff}$ by using impurity puffing, which subsequently affects the rotation direction. Shown in Fig.15 is a comparison of two similar discharges, one with strong argon puffing. While the electron density and temperature are nearly the same, the discharge with the agressive argon puffing has substantially higher $Z_{\rm eff}$ and radiated power, and the core rotation velocity direction changed from counter- to co-current. This behavior is quantified

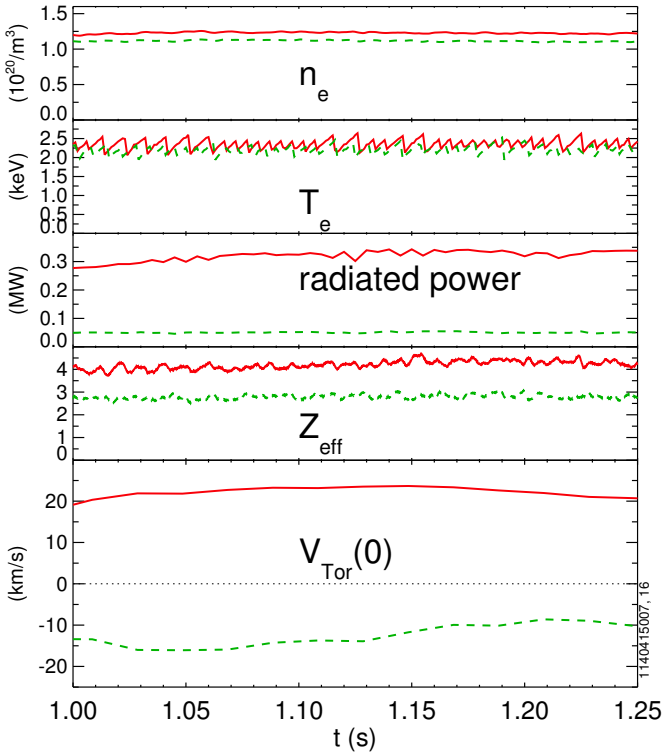

Figure 15: Time history comparison of two 5.5 T, 1.0 MA D discharges with (red) and without (green dashed) strong argon puffing. From top to bottom: the electron density, central electron temperature, radiated power, $Z_{\rm eff}$ and core toroidal rotation velocity.

through a comparison of the rotation velocity in shot by shot density scans, with and without the strong argon puffing. The results are presented in Fig.16. The critical

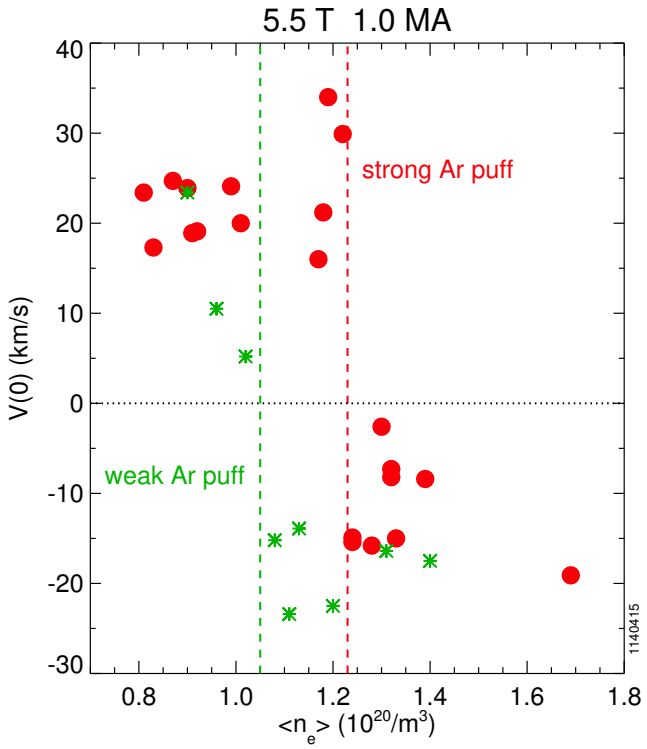

Figure 16: The central toroidal rotation velocity as a function of electron density for 5.5 T, 1.0 MA discharges with (red dots) and without (green asterisks) strong argon puffing.

density for rotation reversal increased from $\sim 1.05\times10^{20}/\mathrm{m}^3$ to $\sim 1.23\times10^{20}/\mathrm{m}^3$ in the plasmas with heavy argon injection. For discharges within this interval, the density and temperatures were similar, but the plasmas with higher Z_{eff}, and therefore higher ν_*, exhibited co-current rotation. A similar result was seen with nitrogen puffing [39]. Ordinarily, an increase in collisionality would lead to a rotation reversal from co- to counter-current, so this result suggests that there are other factors at play beyond simply ν_*. Increasing Z_{eff}, and hence the main ion dilution, may have the effect of stabilizing ITG modes, which ordinarily dominate in the higher density SOC regime [40, 39, 41, 42].

4. Summary and Discussion

Rotation reversals have been observed over a wide range of operating conditions in C-Mod deuterium discharges, with plasma current between 0.40 and 1.57 MA and toroidal magnetic field from 2.9 to 8.1 T. There is a critical density for reversals such that the product of $n_{crit} q_{95} R \sim B_T/2$, where n_{crit} is the critical density ($10^{20}/m^3$), with R in m and B_T in T. This condition is equivalent to $n/n_G \sim 0.15$. Observations from C-Mod have shown the strong correlation between the density at which rotation reversal occurs, the density of the LOC/SOC transition and the fraction of the density limit. Comparisons with the LOC/SOC transition on multiple devices, shown in Fig.9, suggests that the connection with the density limit is not universal. This would seem to be consistent with the observation of the density limit originating in the edge/SOL [33, 43, 44] and rotation reversal as a core phenomenon [4, 5, 6, 8, 9, 11, 12, 15, 1, 22, 23, 17, 19], although some subtle edge-core coupling cannot be strictly ruled out. Evidence pointing to collisionality as a controlling dimensionless parameter for both seems strong, however the appropriate dimensional normalization for the collision frequency deserves more careful study. For example, there has been analysis suggesting that the LOC/SOC transition is linked to electron-ion heat exchange, which leads to a change in the dominant energy loss channel. In that case $\nu_{ie}\tau_E$ might be a better dimensionless parameter than ν_* [41]. An expanded data set could be very useful in answering this question and shedding more light on the underlying mechanism. Understanding of the density limit is still evolving [44], especially for the case of core fueling, as by pellets, and in H-mode. The latter involves an interplay of a back transition from H- to L-mode, followed by a rapid progression to the density limit. For the edge fueled, L-mode density limit, relatively recent experiments indicate that a collapse of the edge shear layer, followed by a surge in turbulence spreading, occurs at the limit.

Similar observations of the relation between rotation reversals and the LOC/SOC transition have been obtained in C-Mod hydrogen and helium plasmas. Modulation experiments have been conducted varying the toroidal magnetic field, electron density and ICRF power (electron temperature). The core rotation velocity is anti-correlated with B_T, but exhibits hysteresis with n_e and T_e, where both co- and counter-current rotation states exist for the same density and temperature. The hysteresis can be unified using the collisionality, with the loop ocurring near a critical value of $\nu_* \sim 0.3$ (evaluated at the q = 1 surface). Agressive argon puffing, with a notable increase in $Z_{\rm eff}$, causes the critical density to increase, which suggests that ν_* alone may not be the relevant parameter. Modeling has suggested that a transition from trapped electron mode (TEM) to ion temperature gradient (ITG) mode dominated core turbulence can explain important aspects of the phenomenology of LOC/SOC confinement, non-diffusive/diffusive transport and co/counter rotation transitions [41, 45, 16, 46, 47]. While such a binary categorization is too broad to capture the details around the transitions (such as the potential importance of sub-dominant modes, mixed modes or profile effects), it is still useful to understand the global parametric dependences and overall trends. Here, the hypothesis is that the transition from co- to counter-current toroidal rotation with heavy argon puffing happens at a higher collisionality because the higher $Z_{\rm eff}$ leads to lower ITG drive at the same collisionality. It is well known that dilution of main ions stabilizes ITG turbulence [40, 39, 42] and therefore higher collisionality is needed for ITG modes to prevail (either through the damping of TEMs *via* collisions

or by an increase in ion temperature gradients when ions and electrons are more tightly coupled in these electron-heating dominated conditions). The details of the effects of impurities on ITG mode stabilization are the keys to understanding this latter effect and additional modeling is needed to confirm this hypothesis, and will be performed as part of future work.

5. Acknowledgements

The authors thank J. Irby and J. Hughes for electron density and temperature measurements, L. Wang and J. Citrin for enlightening discussions, the ICRF group and the entire C-Mod team for expert operation of the device. Work supported at MIT by DoE Award DE-SC0014264.

References

[1] Y. Camenen, C. Angioni, A. Bortolon, B.P. Duval, E. Fable, W.A. Hornsby, R.M. McDermott, D.H. Na, Y.-S. Na, A.G. Peeters and J.E. Rice, 2017 *Plasma Phys. Control. Fusion* **59** 034001.

[2] P.H. Diamond, Y. Kosuga, O.D. Gurcan, C.J. McDevitt, T.S. Hahm, N. Fedorczak, J.E. Rice, W.X. Wang, J.M. Kwon, *et al.*, 2013 *Nucl. Fusion* **53** 104019.

[3] B.P. Duval, B. Joye and B. Marchal, 1992 *Nucl. Fusion* **32** 1405.

[4] A. Bortolon, B.P. Duval, A. Pochelon, and A. Scarabosio, 2006 *Phys. Rev. Lett.* **97** 235003.

[5] B.P. Duval, A. Bortolon, A. Karpushov, R.A. Pitts, A. Pochelon, A. Scarabosio and the TCV Team, 2007 *Plasma Phys. Control. Fusion* **49** B195.

[6] B.P. Duval, A. Bortolon, A. Karpushov, R.A. Pitts, A. Pochelon, O. Sauter, A. Scarabosio, G. Turri the TCV Team, 2008 *Phys. Plasmas* **15** 056113.

[7] J.E. Rice, A.C. Ince-Cushman, M.L. Reinke, Y. Podpaly, M.J. Greenwald, B. LaBombard and E.S. Marmar, 2008 *Plasma Phys. Control. Fusion* **50** 124042.

[8] J.E. Rice, B.P. Duval, M.L. Reinke, Y.A. Podpaly, A. Bortolon, R.M. Churchill, I. Cziegler, P.H. Diamond, A. Dominguez, P.C. Ennever *et al.*, 2011 *Nucl. Fusion* **51** 083005.

[9] J.E. Rice, I. Cziegler, P.H. Diamond, B.P. Duval, Y.A. Podpaly, M.L. Reinke, P.C. Ennever, M.J. Greenwald, J.W. Hughes, Y. Ma, E.S. Marmar, M. Porkolab, N. Tsujii and S. M. Wolfe, 2011 *Phys. Rev. Lett.* **107** 265001.

[10] J.E. Rice, M.J. Greenwald, Y.A. Podpaly, M.L. Reinke, P.H. Diamond, J.W. Hughes, N.T. Howard, Y. Ma, I. Cziegler, B.P. Duval *et al.*, 2012 *Phys. Plasmas* **19** 056106.

[11] J.E. Rice, C. Gao, M.L. Reinke, P.H. Diamond, N.T. Howard, H.J. Sun, I. Cziegler, A.E. Hubbard, Y.A. Podpaly, W.L. Rowan *et al.*, 2013 *Nucl. Fusion* **53** 033004.

[12] R.M. McDermott, C. Angioni, G.D. Conway, R. Dux, E. Fable, R. Fischer, T. Ptterich, F. Ryter, E. Viezzer and the ASDEX Upgrade Team, 2014 *Nucl. Fusion* **54** 043009.

[13] C. Gao, J.E. Rice, H.J. Sun, M.L. Reinke, N.T. Howard, D. Mikkelson, A.E. Hubbard, M.A. Chilenski, J.R. Walk, J.W. Hughes *et al.*, 2014 *Nucl. Fusion* **54** 083025.

[14] J.C. Hillesheim, F.I. Parra, M. Barnes, N.A. Crocker, H. Meyer, W.A. Peebles, R. Scannell, A. Thornton and the MAST Team, 2015 *Nucl. Fusion* **55** 032003.

[15] D.H. Na, Yong-Su Na, S.G. Lee, C. Angioni, S.M. Yang, H.-S. Kim, T.S. Hahm, W.H. Ko, H. Jhang, W.J. Lee *et al.*, 2016 *Nucl. Fusion* **56** 036011.

[16] B.A. Grierson, C. Chrystal, S.R. Haskey, W.X. Wang, T.L. Rhodes, G.R. McKee, K. Barada, X. Yuan, M.F.F. Nave, A. Ashourvan, C. Holland, 2019 *Phys. Plasmas* **26** 042304.

[17] N.M. Cao, J.E. Rice, P.H. Diamond, A.E. White, S.G. Baek, M.A. Chilenski, J.W. Hughes, J. Irby, M.L. Reinke, P. Rodriguez-Fernandez *et al.*, 2019 *Nucl. Fusion* **59** 104001.

[18] G. Shukla, K. Shah, M.B. Chowdhuri, H. Raj, T. Macwan, R. Manchanda, U.C. Nagora, R.L. Tanna, K.A. Jadeja, K. Patel *et al.*, 2019 *Nucl. Fusion* **59** 106049.

[19] N.M. Cao, J.E. Rice, P.H. Diamond, A.E. White, M.A. Chilenski, P.C. Ennever, J.W. Hughes, J. Irby, M.L. Reinke, P. Rodriguez-Fernandez, Alcator C-Mod Team, 2020 *Phys. Plasmas* **27** 052303.

[20] J. Bernardo, C Fenzi, C Bourdelle, Y Camenen, H Arnichand, Joo P S Bizarro, S Cortes, X Garbet, Z O Guimares-Filho, T Aniel *et al.*, 2015 *Plasma Phys. Control. Fusion* **57** 035002.

[21] E. Trier, P. Hennequin, .D. Grcan, R. Sabot, J. Bucalossi, Z.O. Guimares-Filho, C. Bourdelle, F. Clairet, G. Falchetto, C. Fenzi *et al.*, 2017 *Nucl. Fusion* **57** 046021.

[22] Y.J. Shi, J.M. Kwon, P.H. Diamond, W.H. Ko, M.J. Choi, S.H. Ko, S.H. Hahn, D.H. Na, J.E. Leem, J.A. Lee *et al.*, 2017 *Nucl. Fusion* **57** 066040.

[23] D.H. Na, Yong-Su Na, C. Angioni, S.M. Yang, J.M. Kwon, Hogun Jhang, Y. Camenen, S.G. Lee, Y.J. Shi, W.H. Ko *et al.*, 2017 *Nucl. Fusion* **57** 126008.

[24] J.E. Rice, J. Citrin, N.M. Cao, P.H. Diamond, M. Greenwald and B.A. Grierson, 2020 *Nucl. Fusion* **60** 105001.

[25] E.S. Marmar and the Alcator C-Mod Group, 2007 *Fusion Sci. Technol.* **51** 261.

[26] M. Greenwald A. Bader, S. Baek, M. Bakhtiari, H. Barnard, W. Beck, W. Bergerson, I. Bespamyatnov, P. Bonoli, D. Brower *et al.*, 2014 *Phys. Plasmas* **21** 110501.

[27] N.P. Basse, A. Dominguez, E.M. Edlund, C.L. Fiore, R.S. Granetz, A.E. Hubbard, J.W. Hughes, I.H. Hutchinson, J.H. Irby, B. LaBombard *et al.*, 2007 *Fusion Sci. Technol.* **51** 476.

[28] A. Ince-Cushman, J.E. Rice, M. Bitter, M.L. Reinke, K.W. Hill, M.F. Gu, E. Eikenberry, Ch. Broennimann, S. Scott, Y. Podpaly, S.G. Lee, E.S. Marmar, 2008 *Rev. Sci. Instrum.* **79** 10E302.

[29] M.L. Reinke, Y.A. Podpaly, M. Bitter, I.H. Hutchinson, J.E. Rice, L. Delgado-Aparicio, C. Gao, M. Greenwald, K. Hill, N.T. Howard, A. Hubbard, J.W. Hughes, N. Pablant, A.E. White, S.M. Wolfe, 2012 *Rev. Sci. Instrum.* **83** 113504.

[30] S. Ejima, T.W. Petrie, A.C. Riviere, T.R. Angel, C.J. Armentrout, D.R. Baker, F.P. Blau, G. Bramson, N.H. Brooks, R.W. Callis *et al.*, 1982 *Nucl. Fusion* **22** 1627.

[31] J.E. Rice, W.D. Lee, E.S. Marmar, P.T. Bonoli, R.S. Granetz, M.J. Greenwald, A.E. Hubbard, I.H. Hutchinson, J.H. Irby, Y. Lin *et al.*, 2004 *Nucl. Fusion* **44** 379.

[32] Z.S. Hartwig and Y.A. Podpaly, 2011 Magnetic Fusion Energy Formulary, PSFC MIT, Cambridge, MA

[33] M. Greenwald, J.L. Terry, S.M. Wolfe, S. Ejima, M.G. Bell, S.M. Kaye and G.H. Neilson, 1988 *Nucl. Fusion* **28** 2199.

[34] M.F.F. Nave, E. Delabie, J. Ferreira, J. Garcia, D. King, M. Lennholm, B. Lomanowski, F. Parra, P.R. Fernandez, J. Bernardo *et al.*, 2023 *Nucl. Fusion* **63** 044002.

[35] F. Bagnato, B.P. Duval, O. Krutkin, A. Iantchenko and the TCV Team, 2023 *Nucl. Fusion* **63** 056006.

[36] M.L. Reinke, J.E. Rice, A.E. White, M. Greenwald, N.T. Howard, P. Ennever, C. Gao, A.E. Hubbard and J.W. Hughes, 2013 *Plasma Phys. Control. Fusion* **55** 012001.

[37] A.E. White, N.T. Howard, M. Greenwald, M.L. Reinke, C. Sung, S. Baek, M. Barnes, J. Candy, A. Dominguez, D. Ernst, C. Gao *et al.*, 2013 *Phys. Plasmas* **20** 056106.

[38] M.A. Chilenski, M.J. Greenwald, A.E. Hubbard, J.W. Hughes, J.P. Lee, Y.M. Marzouk, J.E. Rice and A.E. White, 2017 *Nucl. Fusion* **57** 126013.

[39] P. Ennever, M. Porkolab, J. Candy, G. Staebler, M.L. Reinke, J.E. Rice, J.C. Rost, D. Ernst, C. Fiore, J. Hughes, J. Terry and the Alcator C-Mod Team, 2015 *Phys. Plasmas* **22** 072507.

[40] M. Porkolab, J. Dorris, P. Ennever, C. Fiore, M. Greenwald, A. Hubbard, Y. Ma, E. Marmar, Y. Podpaly, M.L. Reinke *et al.*, 2012 *Plasma Phys. Control. Fusion* **54** 124029.

[41] I. Erofeev, E. Fable, C. Angioni, R.M. McDermott and The ASDEX Upgrade Team, 2017 *Nucl. Fusion* **57** 126067.

[42] N. Bonanomi, P. Mantica, J. Citrin, C. Giroud, E. Lerche, C. Sozzi, D. Taylor, M. Tsalas, D. Van Eester and JET contributors, 2018 *Nucl. Fusion* **58** 026028.

[43] Greenwald M., 2002 *Plasma Phys. Control. Fusion* **44** R27.

[44] P.H. Diamond, R. Singh, T. Long, R. Hong, R. Ke, Z. Yan, M. Cao and G.R. Tynan, 2023, *Phil. Trans. R. Soc. A* **381** 20210227.

[45] P. Rodriguez-Fernandez, A.E. White, N.T. Howard, B.A. Grierson, G.M. Staebler, J.E. Rice, X. Yuan, N.M. Cao, A.J. Creely, M.J. Greenwald, A.E. Hubbard, J.W. Hughes, J.H. Irby, and F. Sciortino, 2018 *Phys. Rev. Lett.* **120** 075001.

[46] P. Rodriguez-Fernandez, A.E. White, N.T. Howard, B.A. Grierson, X. Yuan, G.M. Staebler, J.E. Rice, C. Angioni, N.M. Cao, A.J. Creely *et al.*, 2019 *Nucl. Fusion* **59** 066017.

[47] P. Rodriguez-Fernandez, A.E. White, N.T. Howard, B.A. Grierson, L. Zeng, X. Yuan, G.M. Staebler, M.E. Austin, T. Odstrcil, T.L. Rhodes, F. Sciortino, J.E. Rice, K.E. Thome, C. Angioni, E. Fable, O. Meneghini, 2019 *Phys. Plasmas* **26** 062503.